Annu. Rev. Mater. Res. 2002. 32:113–40
doi: 10.1146/annurev.matsci.32.112001.132041

PHASE-FIELD MODELS FOR MICROSTRUCTURE EVOLUTION

Long-Qing Chen
Department of Materials Science and Engineering, Penn State University, University Park, Pennsylvania 16802; e-mail: chen@matse.psu.edu

Key Words solidification, phase transformations, grain growth, computer simulation, morphological evolution

■ **Abstract** The phase-field method has recently emerged as a powerful computational approach to modeling and predicting mesoscale morphological and microstructure evolution in materials. It describes a microstructure using a set of conserved and nonconserved field variables that are continuous across the interfacial regions. The temporal and spatial evolution of the field variables is governed by the Cahn-Hilliard nonlinear diffusion equation and the Allen-Cahn relaxation equation. With the fundamental thermodynamic and kinetic information as the input, the phase-field method is able to predict the evolution of arbitrary morphologies and complex microstructures without explicitly tracking the positions of interfaces. This paper briefly reviews the recent advances in developing phase-field models for various materials processes including solidification, solid-state structural phase transformations, grain growth and coarsening, domain evolution in thin films, pattern formation on surfaces, dislocation microstructures, crack propagation, and electromigration.

INTRODUCTION

Microstructures are compositional and structural inhomogeneities that arise during processing of materials. Microstructure evolution is common in many fields including biology, hydrodynamics, chemical reactions, and phase transformations. Materials microstructures may consist of spatially distributed phases of different compositions and/or crystal structures, grains of different orientations, domains of different structural variants, domains of different electrical or magnetic polarizations, and structural defects. These structural features usually have an intermediate mesoscopic length scale in the range of nanometers to microns. The size, shape, and spatial arrangement of the local structural features in a microstructure play a critical role in determining the physical properties of a material.

Microstructure evolution takes place to reduce the total free energy that may include the bulk chemical free energy, interfacial energy, elastic strain energy, magnetic energy, electrostatic energy, and/or under applied external fields such as applied stress, electrical, temperature, and magnetic fields. Due to the complex

and nonlinear nature of microstructure evolution, numerical approaches are often employed. In the conventional approach to modeling microstructure evolution, the regions separating the compositional or structural domains are treated as mathematically sharp interfaces. The local interfacial velocity is then determined as part of the boundary conditions or calculated from the driving force for interface motion and the interfacial mobility. This involves the explicit tracking of the interface positions. Although such an interface-tracking approach can be successful in one-dimensional systems, it becomes impractical for complicated three-dimensional microstructures. During the past ten years, the phase-field approach has emerged as one of the most powerful methods for modeling many types of microstructure evolution processes. It is based on a diffuse-interface description developed more than a century ago by van der Walls (1, 2) and almost 40 years ago independently by Cahn & Hilliard (3). The temporal microstructure evolution is described by a pair of well-known continuum equations, namely, the Cahn-Hilliard nonlinear diffusion equation (4) and the Allen-Cahn (time-dependent Ginzburg-Landau) (5) equation. With random thermal noises, both types of equations become stochastic, and their applications to studying critical dynamics have been extensively discussed (6, 7). Phase-field models describe microstructure phenomena at the mesoscale and contain the corresponding sharp- or thin-interface descriptions as a particular limit [see (8) for a recent discussion]. There are basically two types of applications of phase-field models. In the first type, field variables also called phase-fields, are introduced for the sole purpose of avoiding tracking the interfaces. Essentially all phase-field models of solidification belong to this type. As a matter of fact, the term phase-field model was first introduced in modeling solidification of a pure melt (9–11). The thermodynamic and kinetic coefficients in a phase-field model are then chosen to match the corresponding parameters in the conventional sharp- or thin-interface equations through asymptotic analyses. The development of phase-field models for solidification has recently been reviewed by Karma (12) and Ode et al. (13). In the second type, the field variables correspond to well-defined physical order parameters such as long-range order parameters for order-disorder transformations and the composition fields for phase separation. These types of models assume that the microstructure evolution during a given process is governed by the phase-field equations and, in principle, all the thermodynamic and kinetic coefficients can be related to microscopic parameters. They have been extensively applied to modeling solid-state phase transformations and have also been recently reviewed (14, 15). In addition to solidification and solid-state phase transformations, phase-field models have been proposed for a number of other important materials processes including grain growth and coarsening (16–19), microstructure evolution in thin films (20, 21), surface-stress-induced pattern formation (22), crack propagation (23, 24), crystal growth in the presence of strain (25, 26), dislocation-solute interactions (27, 28), dislocation dynamics (29), electromigration (30, 31), and multicomponent interdiffusion (32). The main purpose of this paper is to give a brief review of the recent applications of the phase-field method.

Phase-Field Method

A phase-field model describes a microstructure, both the compositional/structural domains and the interfaces, as a whole by using a set of field variables. The field variables are continuous across the interfacial regions, and hence the interfaces in a phase-field model are diffuse. There are two types of field variables, conserved and nonconserved. Conserved variables have to satisfy the local conservation condition. In the diffuse-interface description (1–3), the total free energy of an inhomogeneous microstructure system described by a set of conserved ($c_1, c_2, \ldots$) and nonconserved ($\eta_1, \eta_2, \ldots$) field variables is then given by

$$F = \int \left[f(c_1, c_2, \ldots, c_n, \eta_1, \eta_2, \ldots, \eta_p) + \sum_{i=1}^{n} \alpha_i (\nabla c_i)^2 + \sum_{i=1}^{3}\sum_{j=1}^{3}\sum_{k=1}^{p} \beta_{ij} \nabla_i \eta_k \nabla_j \eta_k \right] d^3r + \iint G(r - r')\, d^3r\, d^3r', \qquad 1.$$

where f is the local free-energy density that is a function of field variables c_i and η_i, α_i and β_{ij} are the gradient energy coefficients. The first volume integral represents the local contribution to the free energy from short-range chemical interactions. The origin of interfacial energy comes from the gradient energy terms that are nonzero only at and around the interfaces. The second integral represents a nonlocal term that contains the contributions to the total free energy from any one or more of the long-range interactions, such as elastic interactions, electric dipole-dipole interactions, electrostatic interactions, etc., that also depend on the field variables. The main differences among different phase-field models lies in the treatment of various contributions to the total free energy.

Local Free-Energy Function

One of the key components in a phase-field model is the local free-energy density function. Many of the phase-field models, particularly in solidification modeling, use a double-well form for the function, namely,

$$f(\phi) = 4\Delta f \left(-\frac{1}{2}\phi^2 + \frac{1}{4}\phi^4 \right), \qquad 2.$$

where ϕ is a field variable. The free-energy function has a doubly degenerate minima represented by $\phi = -1$ and $\phi = +1$. For example, in the case of solidification, $\phi = -1$ and $\phi = +1$ represent the liquid and solid states, respectively. Δf is the potential height between the two states with the minimum free energy. If ϕ represents a conserved composition field, the two minima represent the two equilibrium phases with different compositions, and Δf is then the driving force for the transformation of a single homogeneous phase ($\phi = 0$) to a heterogeneous mixture of two phases represented by $\phi = -1$ and $\phi = +1$ during isostructural decomposition. If ϕ is a long-range order parameter field, $\phi = -1$ and $\phi = +1$

describe two thermodynamically degenerate antiphase domain states. For some processes, it may be more desirable to have the two minima of the free energy located at $\phi = 0$ and $\phi = 1$, then the following function, $f(\phi) = 4\Delta f\phi^2(1-\phi)^2$, can be employed.

Another free energy function that has sometimes been employed in phase-field models is the so-called double-obstacle potential,

$$f(\phi) = \Delta f(1-\phi^2) + I(\phi), \qquad 3.$$

where

$$I(\phi) = \begin{cases} \infty & \text{if} \quad |\phi| > 1 \\ 0 & \text{if} \quad |\phi| \le 1 \end{cases}.$$

This potential has a computational advantage that the field variable assumes the value of -1 and $+1$ outside the interfacial region, whereas in the case of the double-well potential (Equation 2), the values of the field variable slowly go to -1 and $+1$ away from the interface. The double-obstacle potential was first introduced by Oono & Puri in their cell-dynamics modeling of pattern evolution during ordering or phase separation of a quenched system (33). It was later used by Blowey & Elliot (34) for modeling spinodal decomposition using the Cahn-Hilliard equation. Recently, this potential has been applied to modeling morphological evolution of voids in metal interconnects (31).

In their phase-field model for dislocation dynamics, Wang et al. (29) introduced the following local free-energy function, so-called the crystalline energy,

$$f(\phi) = \Delta f \sin^2(\pi\phi). \qquad 4.$$

It has an infinite number of minima located at $\phi = -\infty, \ldots, -1, 0, +1, \ldots +\infty$, Δf is the energy barrier between two neighboring minima. In this case, the absolute values of the phase field at the potential minima represent the discontinuous relative displacements between the two lattice planes above and below a slip plane, measured in unit of a given Burgers vector on the slip system, and the positive and negative signs for the phase field describe the opposite directions of the Burgers vectors.

In many applications of the phase-field model to real materials processes, it is often necessary to introduce more than one field variables or to couple one type of field with another. Even in the phase-field model for solidification of a pure liquid, the phase field is coupled to a temperature field, and one of the potentials that has been employed is (35)

$$f(\phi, T) = 4\Delta f\left(-\frac{1}{2}\phi^2 + \frac{1}{4}\phi^4\right) + \frac{15\alpha}{8}\left(\phi - \frac{2}{3}\phi^3 + \frac{1}{5}\phi^5\right)(T - T_m), \qquad 5.$$

where α is a positive constant, and T_m is the equilibrium melting temperature. With the particular functional dependence of the second term on ϕ in Equation 5, the two equilibrium values for ϕ are independent of the undercooling $(T - T_m)$. With

this potential, the driving force ΔG_v, the free-energy difference per unit volume between the solid and the liquid, for solidification at a given temperature T is given by

$$\Delta G_v = f(+1, T) - f(-1, T) = 2\alpha(T - T_m). \quad 6.$$

Another example involving coupling between field variables is a phase-field model for grain growth in which the fields describe the spatial distributions of grains with different orientations. This involves a simple extension of the double-well potential to one with an infinite number of minima (16),

$$f(\phi_1, \phi_2, \ldots) = 4\Delta f\left(-\frac{1}{2}\sum_i \phi_i^2 + \frac{1}{4}\sum_i \phi_i^4\right) + \alpha \sum_i \sum_{j>i} \phi_i^2 \phi_j^2, \quad 7.$$

where α is a positive coefficient, and Δf is the energy barrier among the minimum states. With $\alpha > 2\Delta f$, the infinite number of minima are located at $(1, 0, \ldots)$, $(0, 1, \ldots)$, $(-1, 0, \ldots)$, etc., representing the infinite number of possible orientations of grains in a polycrystal.

For many solid-state phase transformations, the field variables correspond to well-defined physical order parameters. In this case, the local free-energy function is typically expressed as a polynomial of order parameters, using a conventional Landau-type of expansion. All the terms in the expansion are required to be invariant with respect to the symmetry operations of the high-temperature phase. For example, for precipitation of an ordered phase ($L1_2$) from a face-centered-cubic (FCC) matrix in a binary alloy, with expansion terms up to the fourth order, the local free-energy function is given by (36–40)

$$f(c, \eta_1, \eta_2, \eta_3) = f_d(c, T) + \frac{1}{2}A_2(c, T)\left(\eta_1^2 + \eta_2^2 + \eta_3^2\right) + \frac{1}{3}A_3(c, T)\eta_1\eta_2\eta_3 + \frac{1}{4}A_{41}(c, T)\left(\eta_1^4 + \eta_2^4 + \eta_3^4\right) + \frac{1}{4}A_{42}(c, T)\left(\eta_1^2\eta_2^2 + \eta_2^2\eta_3^2 + \eta_1^2\eta_3^2\right), \quad 8.$$

where $f_d(c, T)$ is the free energy of the disordered phase, and A_2, A_3, A_{41}, and A_{42} are the expansion coefficients that are functions of temperature and composition. The free-energy function (Equation 8) has quadruple-degenerate minima with respect to the order parameters. If $A_3(c, T) < 0$, the free energy minima are located at

$$(\eta_0, \eta_0, \eta_0), (\eta_0, -\eta_0, -\eta_0), (-\eta_0, \eta_0, -\eta_0), (-\eta_0, -\eta_0, \eta_0), \quad 9.$$

where η_0 is the equilibrium long-range parameter at a given composition and temperature. The four sets of long-range order parameters given in Equation 9 describe the four energetically equivalent antiphase domains of the $L1_2$ ordered phase related by a primitive lattice translation of the parent disordered FCC phase. The free energy of the ordered phase as a function of composition can be obtained by substituting order-parameter values from Equation 9 into the free-energy function (Equation 8).

The last example is the free-energy function employed in a phase-field model for domain structure evolution during a cubic to tetragonal ferroelectric phase transition. In this case, the local electric polarization fields, (P_1, P_2, P_3) are the natural field variables that describe a domain structure. Assuming a first-order phase transition, the free-energy function as a function of polarization is given by (20, 41–43)

$$\begin{aligned} f(P_1, P_2, P_3) = {} & A_1\left(P_1^2 + P_2^2 + P_3^2\right) + A_{11}\left(P_1^4 + P_2^4 + P^4\right) \\ & + A_{12}\left(P_1^2P_2^2 + P_2^2P_3^2 + P_1^2P_3^2\right) + A_{111}\left(P_1^6 + P_2^6 + P_3^6\right) \\ & + A_{112}\left[P_1^4\left(P_2^2 + P_3^2\right) + P_2^4\left(P_1^2 + P_3^2\right) + P_3^4\left(P_1^2 + P_2^2\right)\right] \\ & + A_{123}P_1^2P_2^2P_3^2, \end{aligned} \qquad 10.$$

where A_1, A_{11}, A_{12}, A_{111}, A_{112}, and A_{123} are the expansion coefficients. The values of these coefficients determine the thermodynamic behavior of the bulk paraelectric and ferroelectric phases, as well as the bulk ferroelectric properties, such as the ferroelectric transition temperature, the stability and metastability of the parent paraelectric phase, the spontaneous polarization and susceptibility as functions of temperature, etc. For example, $A_1 = 1/(2\varepsilon_o\chi)$, where ε_o is the vacuum permittivity, and χ is the dielelectric susceptibility of the material. A negative value for A_1 corresponds to an unstable parent paraelectric phase with respect to its transition to the ferroelectric state. A positive A_1 value indicates either a stable or metastable parent phase, depending on the relations among A_1, A_{11}, and A_{111}. If $A_{11}^2 > 3A_1A_{111}$, the parent phase is metastable, otherwise it is stable. This potential has been employed in modeling the ferroelectric domain evolution in both bulk single crystals (42–44) and in thin films constrained by a substrate (20).

Gradient Energy

Inherent to microstructures is the existence of interfaces. The excess free energy associated with the compositional and/or structural inhomogeneities occurring at interfaces is the interfacial energy. To relate the interfacial energy to the gradient energy terms in a phase-field model, let us consider a simple system that is described by a single field variable, ϕ. The total free energy of a microstructure for such a system, F, is simplified to be (1–3, 45)

$$F = F_{\text{bulk}} + F_{\text{int}} = \int_V \left[f(\phi) + \frac{1}{2}\kappa_\phi(\nabla\phi)^2 \right] dV, \qquad 11.$$

where F_{bulk} and F_{int} are the bulk and interfacial energies, respectively, and κ_ϕ is the gradient energy coefficient. For the case that ϕ is a composition or long-range order-parameter field, the gradient energy coefficient can be expressed in terms of pair-wise interatomic interaction energies (3, 46). Using the double-well free-energy function (Equation 2), it is easy to show that the specific interfacial energy

(interfacial energy per unit area), γ, is given by

$$\gamma = \frac{4\sqrt{2}}{3}\sqrt{\kappa_\phi \Delta f}. \qquad 12.$$

For systems with more than one field variable, the interfacial energies usually have to be evaluated numerically.

Interfacial energies are, in general, anisotropic due to the crystalline nature of solids. The degree of interfacial energy anisotropy can have a significant effect on the growth morphology and equilibrium shape of particles. A number of approaches have been proposed to introduce interfacial energy anisotropy in phase-field models. Because $\gamma \propto \sqrt{\kappa_\phi}$, one of the simplest ways to introduce anisotropy is to make γ and $\sqrt{\kappa_\phi}$ have the same directional ($\nabla\phi/|\nabla\phi|$) dependence. For example, in solidification modeling, a cubic anisotropy of interfacial energy can be introduced by the following directional dependence of the gradient energy coefficient (47, 48),

$$\sqrt{\kappa(\boldsymbol{n})} = a\left[1 + b\left(n_x^4 + n_y^4 + n_x^4\right)\right], \qquad 13.$$

where n_x, n_y, n_z are the x, y, and z components of a unit vector, $\boldsymbol{n}$. Numerical treatment of systems with sharp corners owing to interfacial energy anisotropy was recently discussed by Eggleston et al. (49). It should be pointed out that although this approach is convenient for introducing the interfacial energy anisotropy using the orientational dependence of the gradient energy coefficients, it is difficult to justify physically.

In solid-state phase transformations, the interfacial energy anisotropy can be introduced naturally through the gradient terms. For example, for the precipitation of an ordered $L1_2$ phase from an FCC matrix, the gradient energy terms can be written as (38, 39)

$$\frac{1}{2}\kappa_c\left[\nabla c(\mathbf{r})\right]^2 + \frac{1}{2}\sum_{p=1}^{3}\kappa_{ij}^{\eta}(p)\nabla_i\eta_p(\mathbf{r})\nabla_j\eta_p(\mathbf{r}), \qquad 14.$$

where the gradient energy coefficients, κ_c and κ_{ij}^{η}, can be related to the microscopic interaction energies in a pair-wise interaction model (46):

$$\kappa_c = -\frac{1}{2}\sum_{\boldsymbol{r}} r^2 W(\boldsymbol{r}), \quad \kappa_{ij}^{\eta}(p) = -\frac{1}{2}\sum_{\boldsymbol{r}} r_i r_j W(\boldsymbol{r}) e^{-i\boldsymbol{k}_{\mathrm{op}}\,\cdot\,\boldsymbol{r}},$$

where $\boldsymbol{r}$ is the position vector, r is the magnitude of $\boldsymbol{r}$, r_i is the i^{th} component of $\boldsymbol{r}$, $W(\boldsymbol{r})$ is the effective pair interaction energies, and $\boldsymbol{k}_{\mathrm{op}}$ is the superlattice vector corresponding to the order parameter η_p. The nonzero gradient energy coefficients satisfy the following relationships,

$$\begin{aligned}\kappa_{11}^{\eta}(1) = \kappa_{22}^{\eta}(2) = \kappa_{33}^{\eta}(3) \neq \kappa_{22}^{\eta}(1) = \kappa_{33}^{\eta}(1)\\ = \kappa_{11}^{\eta}(2) = \kappa_{33}^{\eta}(2) = \kappa_{11}^{\eta}(3) = \kappa_{22}^{\eta}(3). \qquad 15.\end{aligned}$$

Finally, to introduce a desired interfacial energy anisotropy, one could also add higher-order gradient energy terms, although they are also difficult to justify physically. For example, it would be necessary to introduce fourth-order terms in order to produce cubic anisotropy (9, 50),

$$\kappa_{ijkl}\left(\frac{\partial^2\phi}{\partial r_i\partial r_j}\right)\left(\frac{\partial^2\phi}{\partial r_k\partial r_l}\right), \qquad 16.$$

where the gradient coefficient κ_{ijkl} is a fourth-rank tensor, r_i is the ith component of the position vector. It is shown that this high-order gradient energy term results in an interfacial energy that does not exhibit cusps, and hence the equilibrium particle shapes do not contain planar facets (51). However, the resulting interfacial energy anisotropy may be sufficient to produce corners in the Wulff shapes.

Elastic Energy, Electrostatic Energy, Magnetic Energy

Phase transformations in solids usually produce coherent microstructures at their early stages. In a coherent microstructure, the lattice planes and directions are continuous across the interfaces, and the lattice mismatch between phases and domains are accommodated by elastic displacements. The elastic energy contribution to the total free energy in a phase-field model can be introduced directly by expressing the elastic strain energy as a function of field variables or by including coupling terms between the field variables and the displacement gradients in the local free-energy function (52). The relationship between the two approaches was recently discussed (53).

Consider a rather general microstructure described by a conserved composition field c(**r**) and a nonconserved order parameter field $\eta(r)$. Let us assume that the local stress-free strain is linearly proportional to the composition field and has a quadratic dependence on the order parameter field, i.e.,

$$\varepsilon^o_{ij}(r) = \varepsilon^c_{ij}c(r) + \varepsilon^\eta_{ij}\eta^2(r). \qquad 17.$$

It should be emphasized that the linear dependence of stress-free strain on composition is assumed simply for convenience. The elastic energy of a system with a nonlinear dependence of lattice parameter on composition can be obtained using the same approach (53). The stress-free strain (Equation 17) contains two pieces of information: One is the microstructure described by the field variables, $c(r)$ and $\eta(r)$, and the other is the crystallographic relationship between the phases or domains in a microstructure through the lattice expansion coefficients with respect to composition and order parameter, i.e. ε^c_{ij} and ε^η_{ij}. The local elastic stress in a coherent microstructure is then given by

$$\sigma_{ij}(r) = \lambda_{ijkl}(r)\varepsilon^{el}_{kl}(r) = \lambda_{ijkl}(r)\left[\varepsilon_{kl}(r) - \varepsilon^c_{ikl}c(r) - \varepsilon^\eta_{kl}\eta^2(r)\right], \qquad 18.$$

where $\lambda_{ijkl}(r)$ is the elastic modulus tensor, which is, in general, spatially dependent, or inhomogeneous, $\varepsilon_{kl}(r)$ is the total local strain, which is obtained by solving

the following mechanical equilibrium equation,

$$\frac{\partial \sigma_{ij}}{\partial r_j} = 0, \qquad 19.$$

subject to appropriate mechanical boundary conditions. With the elastic solution, $\varepsilon_{kl}(r)$, the total elastic energy of a microstructure can be calculated through the usual expression,

$$E = \frac{1}{2} \int_V \lambda_{ijkl}(r) \varepsilon_{ij}^{el} \varepsilon_{kl}^{el} \, dV. \qquad 20.$$

In the presence of external stress, the mechanical energy contribution to the total free energy becomes

$$E = \frac{1}{2} \int_V \lambda_{ijkl}(r) \varepsilon_{ij}^{el} \varepsilon_{kl}^{el} \, dV - \int_V \sigma_{ij}^{a}(r) \varepsilon_{ij}(r) \, dV, \qquad 21.$$

where σ_{ij}^{a} is the applied stress and can be inhomogeneous.

To solve the mechanical equilibrium equation (Equation 19), most existing phase-field simulations assume homogeneous elasticity where the elastic modulus difference between different phases is neglected, i.e., $\lambda_{ijkl}(r) = \text{constant}$ (14, 15). In this case, the elastic fields can be analytically evaluated for any arbitrary microstructures as shown by Khachaturyan more than 30 years ago (46, 54). There have been significant efforts in incorporating the elastic inhomogeneity through the dependence of the elastic modulus tensor on field variables. When the elastic inhomogeneity is small, first-order approximations may be employed (52, 55, 56). Recently, it was shown that it is possible to incorporate high-order approximations for solving the inhomogeneous elasticity equation using an iterative approach, thus allowing strong elastic inhomogeneity (57). The unique feature of this iterative approach is the fact that the accuracy can be successively improved by using increasingly higher-order approximations without a significant increase in the computational time compared with the homogeneous approximation. Finally, one can always resolve to use direct numerical methods for solving the elastic equation using, e.g., a conjugate gradient method (CGM) (58, 59) or a finite-element method (31). However, such direct numerical solutions are usually more time consuming than those using more approximate methods.

For modeling solid-state phase transformations or other processes that involve charged species or electrical or magnetic dipoles, the electrostatic or magnetic energy contributions to the total free energy of a microstructure can be evaluated using an approach similar to that of elastic energy. The electrical or magnetic field distribution in a microstructure has to be solved first for any distribution of charges and dipoles, and the total electrostatic or magnetic energy is then expressed as a functional of the field variables. For example, using the simplest approximation, i.e., the dielectric or magnetic susceptibility is a constant, the electrostatic or

magnetic energy of a domain structure is (44, 46, 60)

$$E_{ele} = \frac{1}{2\varepsilon_o} \int \frac{d^3\mathbf{g}}{(2\pi)^3} |\boldsymbol{P}(\mathbf{g}) \cdot \mathbf{n}|^2 \quad \text{or} \quad E_{mag} = \frac{1}{2\mu_o} \int \frac{d^3\mathbf{g}}{(2\pi)^3} |\boldsymbol{M}(\mathbf{g}) \cdot \mathbf{n}|^2, \qquad 22.$$

where ε_o and μ_o are the permittivity and permeability of vacuum, respectively. P(**g**) and M(**g**) are the Fourier transformations of the electric and magnetic dipole distributions, P(**r**) and M(**r**), which are the natural field variables for ferroelectric and magnetic materials. For more general cases in which the dielectric and magnetic properties are inhomogeneous, the electrostatic and magnetic equilibrium equations have to be solved numerically with appropriate boundary conditions.

Evolution Equations and Numerical Methods

With the total free energy of a microstructure discussed above, the evolution of field variables in a phase-field model can be obtained by solving the following Cahn-Hilliard (5) and Allen-Cahn (4) equations,

$$\frac{\partial c_i(\mathbf{r}, t)}{\partial t} = \nabla M_{ij} \nabla \frac{\delta F}{\delta c_j(\mathbf{r}, t)} \qquad 23.$$

$$\frac{\partial \eta_p(\mathbf{r}, t)}{\partial t} = -L_{pq} \frac{\delta F}{\delta \eta_q(\mathbf{r}, t)}, \qquad 24.$$

where M_{ij} and L_{pq} are related to atom or interface mobility, $c_1, c_2, \ldots$ are conserved fields, and $\eta_1, \eta_2, \ldots$ are nonconserved.

Modeling the microstructure evolution using the phase-field approach is then reduced to finding solutions to the kinetic Equations 23 and 24. A number of numerical methods have been implemented. Most phase-field simulations employed the simple second-order finite-difference method on a uniform spatial grid and explicit time-stepping. It is well known that in such an explicit scheme, the time step has to be small to keep the numerical solutions stable.

With periodic boundary conditions, one of the techniques often employed is the fast Fourier transform method, which converts the integral-differential equations into algebraic equations [see for example (61–63)]. Alternatively, one can first convert the integral-differential equations to finite difference equations, which are then transformed to the Fourier space. However, in this case, the accuracy in the space discretization is only second-order instead of the spectral accuracy. In the reciprocal space, the simple forward Euler differencing technique can be employed for the time-stepping. The disadvantage of this single-step explicit Euler method is that, although the spatial discretization enjoys the spectral accuracy, it is again only first-order accurate in time, and the numerical stability is still a concern.

Recently, more efficient and accurate semi-implicit Fourier-spectral algorithms have been applied to solving phase-field equations, including those with variable coefficients (64, 65). These algorithms are much more efficient and accurate than the conventional forward Euler method. The semi-implicit schemes can also be

efficiently applied to the phase-field equations with Dirichlet, Neumann, or mixed boundary conditions by using the fast Legendre- or Chebyshev-spectral methods developed (66, 67) for second- and fourth-order equations. However, because the spectral method typically uses a uniform grid for the spatial variables, it may be difficult to resolve extremely sharp interfaces with a moderate number of grid points. In this case, an adaptive spectral method may be more appropriate.

Real-space adaptive grid algorithms have been developed for solving the phase-field equations applied to solidification (68, 69). It has been shown that the number of variables in an adaptive method is significantly reduced compared with those using a uniform mesh. This allows one to solve the field model in much larger systems and for longer simulation times. However, such an adaptive method is in general much more complicated to implement than uniform grids.

Recently, Plapp & Karma proposed an interesting multiscale diffusion Monte Carlo (DMC) algorithm (70) to evolve the large-scale diffusion field outside a thin liquid layer surrounding the interface during solidification modeling. Inside this layer and in the solid, the diffusion equation is solved using a standard finite difference method that is interfaced with the DMC algorithm using the local conservation law for the diffusing quantity. Using this algorithm in a phase-field simulation of solidification of a pure melt, they claimed that it is possible to accurately simulate the three-dimensional dendritic growth at low undercoolings, while achieving a similar efficiency as the adaptive finite-element method.

APPLICATIONS

Existing phase-field applications have been focused on the three major materials processes: solidification, solid-state phase transformation, and grain growth and coarsening. Very recently, a number of new phase-field models have been developed for modeling thin films and surfaces, dislocation dynamics, crack propagation, and electromigration. Examples of existing phase-field applications are summarized in Table 1.

Solidification Modeling

Solidification is the transformation of a liquid to a crystalline solid when the liquid is cooled below the equilibrium melting temperature (T_m). Its fundamental understanding has technological importance in many practical processes such as casting, crystal growth, and welding. The idea of using a phase-field approach to modeling solidification processes was introduced almost 20 years ago (9–11). It was motivated by the desire to predict the complicated dendritic patterns during solidification without explicitly tracking the solid-liquid interfaces. Its success was first demonstrated by Kobayashi (47), who simulated realistic three-dimensional dendrites using a phase-field model for isothermal solidification of a single-component melt. Since then, enormous research effort has been devoted to developing phase-field models for solidifications, and important progress has been made [see (12, 13)

TABLE 1 Applications of the phase-field method

	References
Solidification	
Pure liquid	(9–11, 47, 48, 109, 113, 192)
Pure liquid with fluid flow	(69, 73–84)
Binary alloys	(85–96)
Multicomponent alloys	(98, 103–107)
Nonisothermal solidification	(108)
Solid-State Phase Transformations	
Spinodal phase separation	(52, 55, 56, 61, 120)
Precipitation of cubic ordered intermetallic precipitates from a disordered matrix	(39, 40, 121, 122)
Cubic-tetragonal transformations	(62, 125–129)
Hexagonal to orthorhombic transformations	(130–133)
Ferroelectric transformations	(20, 42, 43, 60, 134)
Phase transformations under an applied stress	(40, 136, 138–140)
Martensitic transformations in single and polycrystals	(135–137)
Coarsening and Grain Growth	
Coarsening	(56, 78, 120, 159, 160)
Grain growth in a single-phase solid	(16–18, 143, 145, 146, 154)
Grain growth in a two-phase solid	(148, 161–163, 165)
Anisotropic grain growth	(155, 156)
Other Applications	
Phase transformations in thin films	(20, 21, 27, 166)
Surface-stress induced pattern formation	(22, 167)
Spiral growth	(168)
Crystal growth under stress	(26, 169, 170)
Solute-dislocation interactions	(27, 28, 173)
Dislocation dynamics	(29, 174–177; S.Y. Hu & L.Q. Chen, unpublished data)
Crack propagation	(23, 24)
Electromigration	(30, 31, 179)

for a more detailed summary on phase-field modeling of solidification]). For example, phase-field models have been developed that can automatically generate side-branching of dendrites by including thermal noises (71). Figure 1 shows an example of a three-dimensional dendritic structure obtained from a phase-field simulation of solidification of a pure Ni melt, taking into account the effect of thermal noises (72). The crystal has a cubic anisotropy with the anisotropic interfacial thermodynamic and kinetic parameters from atomistic simulations. The effect of fluid flow on the dendrite formation has been considered by many groups (69, 73–84). A number of phase-field models have been

proposed for binary alloy systems and have been used in solidification microstructure modeling (85–96). The main difference in models for binary alloys is in the construction of the local free-energy functions. They have been employed to study the dendrite formation during solidification of a binary melt into two- or three-phase mixtures through eutectic (17, 97–100) or peritectic reactions (17, 83, 101, 102). Phase-field models for model ternary alloys (98, 103, 104) and multicomponent systems have been constructed (103, 105–107). There has also been an attempt to develop a phase-field model for the nonisothermal solidification of alloys (108).

Because the sharp-interface equations for solidification are reasonably well established, and the purpose of introducing phase-fields is simply to avoid the moving boundary problem, there have been many efforts to establish the relationship between the phase-field models and the corresponding sharp-interface descriptions [for examples, see (86, 96, 97, 109–116)]. In particular, Karma & Rappel (117) developed a thin-interface analysis (as opposed to the traditional sharp-interface analysis) by taking into account the temperature field variation across the interfacial thickness. They showed that, with the phase-field kinetic parameter obtained from a thin-interface analysis, it is possible to quantitatively model the kinetics of solidification at low undercoolings without a severe restriction on the interfacial width (113). This thin-interface limit analysis has been extended to phase-field models of binary and multicomponent alloys by considering the chemical potential variation across the interface (96, 105, 114, 118). A refined thin-interface analysis of phase-field models for solidification of binary alloys (119) was recently performed by simultaneously considering the dramatically different diffusion coefficients in solid and liquid, the interface stretching correction to the heat conservation condition at the interface, the surface diffusion correction, and the corrections due to the chemical potential variation over the interfacial region. A method for systematically deriving the sharp- or thin-interface equations from phase-field models with more general free-energy functions was recently discussed by Elder et al. (8).

Solid-State Phase Transformations

Phase-field models have been developed for a wide variety of diffusional and diffusionless solid-state phase transformations [for brief reviews, see (14, 15)]. Examples include isostructural phase separation (52, 55, 56, 61, 120), precipitation of an ordered intermetallic phase from a disordered matrix (39, 40, 121–124), cubic to tetragonal transformations (62, 125–129), hexagonal to orthorhombic transformations (130–133), ferroelectric transformations (20, 42–44, 60, 134), proper and improper martensitic transformations in single and polycrystals (135–137), and phase transformations under an applied stress (40, 136, 138–140). The main idea behind the phase-field modeling of solid-state phase transformations is to assume that the free energy of a system can be expressed as a function of physically defined order parameters using Landau-type expansions (see Equations 8 and 10 for examples), and the evolution of these order parameters follows the Allen-Cahn

and Cahn-Hilliard equations. As a matter of fact, for the case of diffusional order-disorder and compositional phase separation processes, it is possible to derive the phase-field equations from the corresponding microscopic equations (39, 141). A unique feature to the solid-state phase transformations is the fact that essentially all microstructures produced from the early stages of a transformation are coherent microstructures. The formation of coherent microstructures involves the generation of elastic strain energy whose magnitude depends on the degree of lattice mismatch, the elastic properties, and the shape and spatial distributions of coherent particles or domains (46). While the bulk chemical free energy depends only on the volume fraction of each phase, the elastic energy is a function of both the volume fraction and morphologies of the coexisting phases. Therefore, the elastic energy often plays a dominant role in the microstructure evolution in coherent systems. It is not surprising that many of the phase-field applications to solid-state transformations are concerned with the elastic strain effect. As an example, a hexagonal-to-orthorhombic transformation is considered (123, 130, 132, 142). The transformation process is described by a compositional and a three-component order parameter field. The orthorhombic phase has three orientation variants, all of which are energetically equivalent and thus have the same probability to form from the parent phase. Three typical microstructures predicted from the simulations are shown in Figure 2*a–c*, representing different volume fractions ($\sim$37, $\sim$67, and 100%) of the orthorhombic phase. In Figure 2*a,b*, four different shades of gray correspond to variant 1, parent phase, variant 2, and variant 3, respectively, with decreasing brightness, whereas in Figure 2*c*, the three variants are presented by different gray levels. There is a significant variation of precipitate morphology with the volume fraction. For the case of 37% volume fraction of the orthorhombic phase, the dominant morphology of precipitates is plate-like with spear-like ends. Here the precipitates prefer to aggregate together forming twin boundaries, which results in very inhomogeneous spatial distribution. For the 67% volume fraction (Figure 2*b*), most of the precipitates have rectangle/square shapes, although the interfacial energy is assumed to be isotropic in the simulation. The majority of the interfaces are interphase boundaries, with very few twin boundaries. Interestingly, in this case, the parent phase evolves into dispersed polygon-shaped particles (triangles, trapezia, irregular pentagons, or hexagons) connected through corners. For the single domain structure (Figure 2*c*), the domain boundaries between different orientation variants are twin boundaries that possess strain compatibility and minimize the elastic strain energy. It is quite remarkable that the phase-field approach combining the macroscopic elasticity theories (46, 54) was able to predict such complex microstructures and their volume fraction dependence, as shown in Figure 2.

Grain Growth

Both solidification and solid-solid phase transformations are driven by the reduction in bulk free energy, whereas coarsening and grain growth take place to reduce

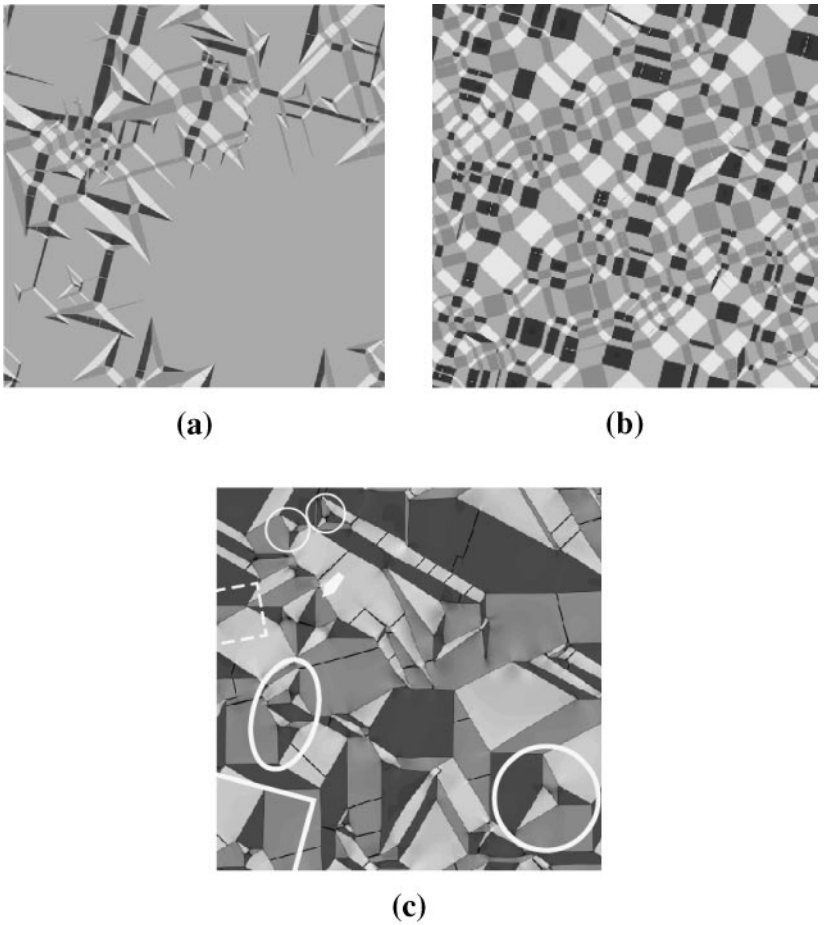

Figure 2 Morphologies of orthorhombic precipitates in a hexagonal matrix at three representative volume fractions obtained from two-dimensional phase-field simulations (along the basal plane of the hexagonal phase) (123). (*a*) 37% volume fraction; (*b*) 67% volume fraction; (*c*) 100% volume fraction, i.e., single-phase orthorhombic domain structure. In (*a*) and (*b*), four different shades of gray correspond to variant 1, parent phase, variant 2, and variant 3, respectively, with decreasing brightness; (*c*) the three variants are presented by different gray levels.

the total interfacial free energy of a microstructure. Several phase-field models have been proposed to describe grain growth. The first model was proposed by Chen & Yang (16), in which the grains of different crystallographic orientations are represented by a set of nonconserved order parameter fields. The evolution of the order parameter fields is described by the Allen-Cahn equations. This model

has been extensively applied to simulating grain growth kinetics in two- (143–145) and three-dimensional systems (146). A similar multiorder parameter model, the so-called multiphase-field model, for grain growth was proposed by Steinbach (17, 147–149). The main difference between the two models is in the fact that the model in (17) imposes the following constraint for the order parameters, $\sum_i \eta_i = 0$, i.e., the sum of all order parameters at a given point is 1.0. The physical interpretation of this constraint is that the order parameters represent the volume fraction of grains of different orientations. Recently, an interesting phase-field model was proposed to study the crystalline grains (19, 150–154). Different from the multiorder parameter models for grain growth, it uses two order parameters to describe a grain structure; one represents the crystalline order; the other reflects the predominantly local orientation of the crystal. Whereas the relaxation of the local orientation order parameter simulates the grain rotation, which is absent from the multiorder parameter models, this order parameter is undefined in a disordered liquid state. Effect of grain boundary energy and mobility anisotropy on grain growth has been studied (155, 156) by modifying the multiorder parameter model (16). In addition to grain growth in single-phase materials, phase-field models have been developed for studying the diffusion-induced grain boundary migration (157), the grain growth kinetics under the influence of solute drag (158), the coarsening kinetics of high-volume fraction of a dispersed phase in a continuous matrix (159, 160), and the kinetics of coupled grain growth and Ostwald ripening in two-phase systems (161–165).

A sequence of grain structure evolution from a recent three-dimensional simulation is shown in Figure 3 (146). It was obtained using a multiorder parameter free-energy model (Equation 7) with 25 order parameters. A dynamic grain-orientation reassignment was developed to minimize the effect of grain coalescence due to the finite number of order parameters employed in the simulation. The Allen-Cahn equations were solved on a 170^3 uniform grid using a finite-difference method. The initial state was generated by assigning small random order-parameter values $\{|\eta_q|\} < 0.001$. This state crystallizes fully within the first few hundred time steps ($\sim$300) to a dense packing of a few thousand grains. With increasing simulation time, grains are eliminated via boundary migration, and owing to the conservation of total volume, the average grain size increases steadily. The average size of grain increases with time with a value for the growth exponent m of 2, as expected for curvature-driven grain boundary migration. With the temporal microstructure evolution, all the statistical information about the microstructure, such as average grain size, size distribution, average number of sides, side distribution, and local topological changes, can be obtained.

Phase Transformations in Thin Films and on Surfaces

There have been a number of applications of the phase-field method to the morphological pattern formation in thin films and on surfaces. For example, Li et al. developed a phase-field model for predicting the coherent domain evolution in

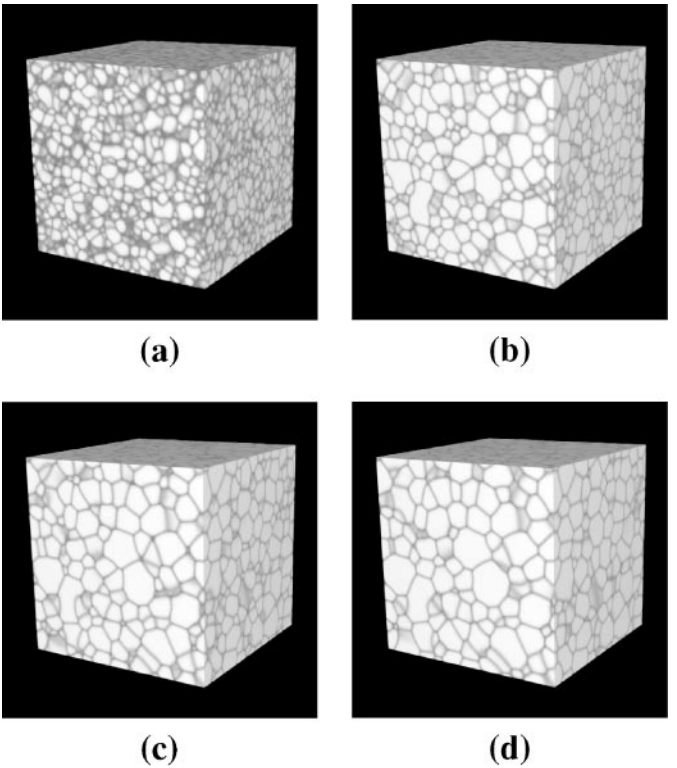

Figure 3 A typical grain evolution process obtained from a three-dimensional phase-field simulation of grain growth assuming isotropic grain boundary energy and isotropic boundary mobility (146). Twenty-five order parameters were used, and an orientation reassignment algorithm was implemented. (*a*) $t^* = 250$; (*b*) $t^* = 1000$; (*c*) $t^* = 1500$; (*d*) $t^* = 2010$, where t^* is the time in reduced unit.

constrained thin films (20, 166). It employs an analytical elastic solution derived for a constrained film with arbitrary eigenstrain distributions. The model is able to predict simultaneously the effects of substrate constraint and temperature on the volume fractions of domain variants, domain-wall orientations, domain shapes, and their temporal evolution during a ferroelectric phase transformation. Figure 4 shows examples of domain structures of a $PbTiO_3$ single crystal film with (001) orientation, coherent-bonded to a (001) cubic substrate. The three drastically different domain structures result from different substrate constraints ranging from compressive to tensile. Leo & Johnson proposed a phase-field model to study the microstructure evolution and long-time coarsening behavior of a thin film attached to a compliant substrate (21). In particular, they studied the spinodal decomposition and coarsening of a thin-film binary alloy using the Cahn-Hilliard equation. Suo &

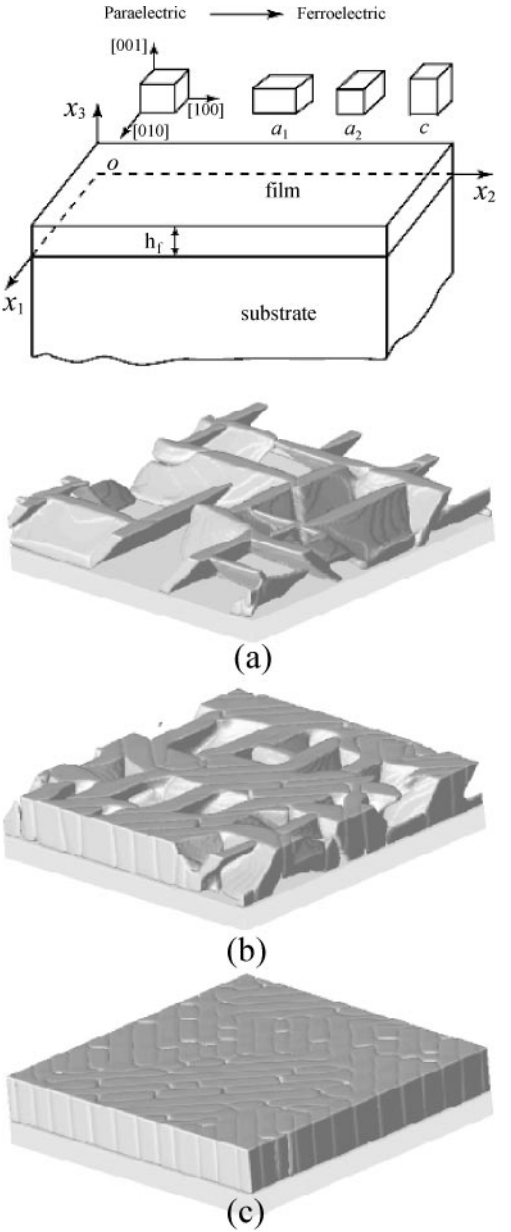

Lu investigated the self-assembly dynamics of a two-phase monolayer on an elastic substrate by incorporating an anisotropic surface stress into a phase-field model of spinodal decomposition (22, 167). The competition between short-range attractive interactions that are responsible for the interfacial energy and long-range repulsive elastic interactions that produce the surface stress results in nanoscale morphological patterns such as interwoven stripes, parallel stripes, triangular lattice of dots, and herringbone structures. Karma & Plapp constructed a phase-field model for spiral surface growth in the step-flow regime where desorption of adatoms is negligible, and the ridge dynamics is governed by the nonlocal diffusion field of adatoms on the whole surface (168). With this model, it is possible to make quantitative predictions for the selected step spacing as a function of the deposition flux, as well as for the dependence of the relaxation time to steady-state growth on the screw dislocation density. Finally, phase-field models for solid-liquid interfaces under stress have been proposed (26, 169, 170). Simulations of a solid subject to uniaxial stress using a phase-field model were able to reproduce the Asaro-Tiller-Grinfeld instability and a transition to fracture (26).

Dislocation Microstructures

It has long been recognized that structural defects such as dislocations play an important role in the diffusional processes and phase transformations in solids. For example, the interaction between composition and a dislocation results in solute segregation and depletion, leading to the formation of so-called Cottrell atmosphere (171). The existence of dislocations may promote the nucleation of a new phase (172). Leonard & Desai were the first to consider the effect of dislocations on the spinodally decomposed two-phase morphologies in a diffuse-interface context (27). Recently, Hu & Chen proposed a diffuse-interface field model by coupling the Cahn-Hilliard diffusion equation with the elastic fields produced from coherent compositional inhomogeneities, as well as from more general structural defects including dislocations (28, 173). This model can easily incorporate elastic anisotropy and allows arbitrary distribution of composition and dislocations. The unique feature of this model is that the elastic fields from dislocations and coherent compositional inhomogeneity are obtained within exactly the same formulation

←

Figure 4 Three representative domain structures in a (001)-oriented $PbTiO_3$ thin film constrained by a (001)-oriented cubic substrate under different degrees of lattice mismatch between the film and the substrate (20, 166). (*a*) The film is under a compressive strain (−0.002); (*b*) the film is under relatively small tensile strain (0.006); (*c*) the film is under a large tensile strain (0.016). Only the a_1- (the tetragonal axis is along the plane of the film) and a_2- (the tetragonal axis is also along the plane of the film but perpendicular to that of a_1 domains are shown. The rest of the film belongs to the c-domain (the tetragonal axis is along the normal to the film).

using the concept of eigenstrains in micromechanics, which is different from the work of Leonard & Desai who directly introduced the analytical elastic solution of a dislocation (27). A similar model was developed by Rodney et al. (174) who introduced two length scales in the simulations to account for the fact that dislocation cores are much smaller than the grid spacing. A significant advance in phase-field modeling of dislocation dynamics was made by Wang et al. (29, 175, 176). They proposed to describe a multidislocation system using a set of order parameters that describe the discontinuous relative displacements between the two lattice planes below and above the slip plane, measured in units of Burgers' vectors. The evolution of the order parameter fields is obtained by solving the Allen-Cahn equation (29, 175, 176). The model not only takes into account the long-range strain-induced interactions among individual dislocations but also automatically incorporates the effects of short-range interactions, such as multiplication and annihilation of dislocations. Figure 5 shows an example from a phase-field simulation of plastic deformation of a model FCC alloy under a uniaxial tensile stress. The dislocation generation during deformation was provided by randomly placed Frank-Read sources in the system. The model has since been extended to polycrystals (177) and to systems with simultaneously evolving phase and dislocation microstructures (174; S.Y. Hu & L.Q. Chen, unpublished data).

Crack Propagation

The application of the phase-field approach to the challenging problem of crack propagation in amorphous solids has recently been explored by Aranson et al. (23) and Karma et al. (24). A nonconserved phase field is introduced to characterize the local state of matter, either the local density or the degree of atomic bonds broken in the solid. For example, the value of 1 for the phase field represents the solid regions, and 0 represent the cracks where the density is zero (23) or where all the atomic bonds are broken (24). At the crack surface, the phase field varies from 0 to 1. The Allen-Cahn equation for the phase field is coupled to the elastodynamics equation for the displacement field. While the evolution of the displacement fields is driven by the applied stress or strain, the evolution of the phase field is determined by a local criterion: Either the local density is below a certain critical density (23) or the local strain is above a critical value (24). Simulations of steady-state crack motion in a strip geometry using the phase-field approach seem to capture the main phenomenological features of crack propagation observed experimentally, although the quantitative modeling of the crack propagation dynamics requires further development.

Electromigration

A phase-field model has been developed to study the motion and evolution of voids in interconnects by electromigration (30, 179). Electromigration is a process in which metal ions drift as a result of electron impact when an electrical current

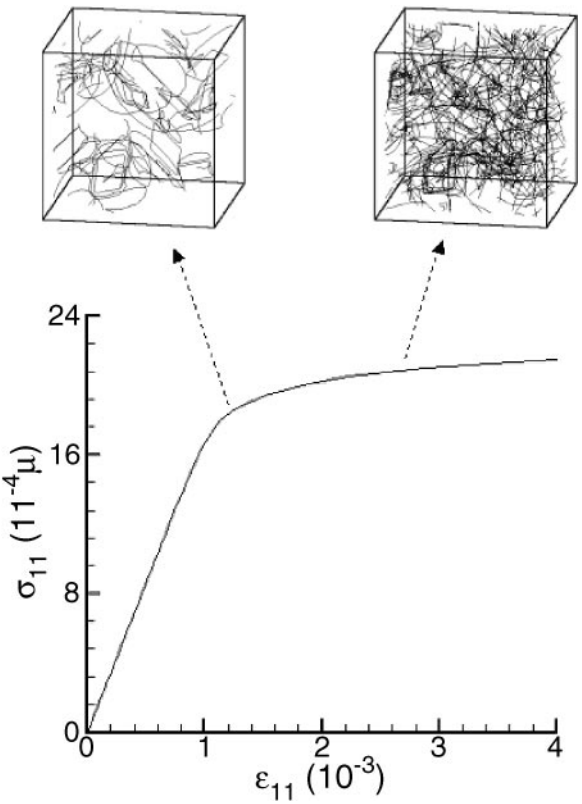

Figure 5 The stress–strain curve obtained from a three-dimensional phase-field simulation of an FCC crystal under a uniaxial loading (σ_{11}) (29, 175, 176). Plastic behavior is reproduced, and the dislocation multiplication with increasing strain (ε_{11}) is illustrated by the three-dimensional dislocation structures corresponding to different strain stages. μ is the shear modulus of the crystal (courtesy of A. Khachaturyan).

passes through a metal thin film or metal wire. A continuously varying conserved order parameter is used to describe the metal and void distributions within the metal film or wire. The time evolution of the metal-void interface is given by two partial differential equations: the Cahn-Hilliard equation for the conserved order parameter and the Laplace's equation for the electrical potential. More recently, Bhate et al. (31) developed a more comprehensive phase-field model by coupling the elasticity equation to the phase-field and electrostatic equilibrium equations to study the void evolution under the simultaneous influence of electrical field and stress. An asymptotic analysis of the equations demonstrates that the zero-level set of the order parameter tracks the motion of a void evolving by diffusion under the coupled effects of stresses and the "electron wind" force.

ROLE OF PHASE-FIELD APPROACH IN MULTISCALE MODELING

It is well known that many materials processes take place over a wide range of length and time scales. Although innovative multiscale modeling approaches have recently been proposed (180–186) for modeling multiple scale processes in many complex multicomponent materials systems, the straightforward information passing from one scale to another is still the main approach in the foreseeable future. Here the phase-field method can provide the critical link between the atomic level fundamental calculations and the macroscopic constitutive modeling. A number of efforts have been made in this direction. For example, a combined first-principles and phase-field methodology has been applied to the problem of θ' (Al_2Cu) precipitation in Al alloys (187, 188). θ' precipitates not only occur in binary Al-Cu alloys but are strengthening precipitates in a wide variety of industrial Al alloys as well. All the necessary thermodynamic information, including the bulk free energies of matrix and precipitate phases, the interfacial energy and its anisotropy, and the lattice mismatch, was obtained from first-principles calculations combined with cluster expansions. Thus it is possible to predict the precipitate shapes using a phase-field model with only the thermodynamic information obtained from first-principles. More quantitative microstructure information, which is useful in understanding precipitation hardening behavior, can be obtained from these phase-field simulations. Atomistic calculations have also been employed to obtain the fundamental properties of solid-liquid interfaces, such as interfacial energies and mobilities, as well as their anisotropies (189, 190), for input to phase-field simulations (72).

For complex multicomponent systems, a number of efforts have been reported in connecting phase-field models with existing thermodynamic and kinetic databases (103, 106, 107). It is possible to directly construct the free-energy function of a phase-field model from existing databases using the CALPHAD method (191). The compositional dependence of atomic mobilities from databases can also be incorporated. However, in order to take into account the effect of elastic energy in solid-state processes, additional databases, such as the crystallographic lattice parameters and elastic constants, have to be constructed. With independently assessed reliable databases, it will be possible to predict the microstructure evolution in complex multicomponent alloys using the phase-field method.

SUMMARY

Phase-field models have been successfully applied to various materials processes including solidification, solid-state phase transformations, coarsening, and growth (Table 1). With the phase-field approach, one can deal with the evolution of arbitrary morphologies and complex microstructures without explicitly tracking the positions of interfaces. This approach can describe different processes such as phase transformations and particle coarsening within the same formulation, and it

is rather straightfoward to incorporate the effect of coherency and applied stresses, as well as electrical and magnetic fields. Future efforts are expected to focus on the exploration of novel applications of the phase-field method to various materials problems, e.g., problems involving simultaneous long-range elastic and electric or magnetic dipole-dipole interactions, low-dimensional systems such as thin films and multilayer structures, and interactions between phase and defect microstructures such as random defects and dislocations. There will also be increasing efforts in establishing schemes to obtain the phase-field parameters directly from more fundamental first-principles electronic structure or atomic calculations. For practical applications, significant additional efforts are required to develop approaches for connecting phase-field models with existing or future thermodynamic, kinetic, and crystallographic databases.

ACKNOWLEDGMENTS

The author is grateful for the continuing financial support from National Science Foundation under grant number DMR-0103354. He thanks Professors Alain Karma, Armen G. Khachatuyran, and Yunzhi Wang for useful discussions on many occasions and for allowing the author to use their figures in this paper. He also thanks V. Vaithyanathan and Shenyang Hu for reading the manuscript before submission.

The *Annual Review of Materials Research* is online at http://matsci.annualreviews.org

LITERATURE CITED

1. Rowlinson JS. 1979. *J. Stat. Phys.* 20:197
2. van der Waals JD. 1894. *Z. Phys. Chem.* 13:657
3. Cahn JW, Hilliard JE. 1958. *J. Chem. Phys.* 28:258–67
4. Cahn JW. 1961. *Acta Metall.* 9:795–801
5. Allen SM, Cahn JW. 1977. *J. Phys.* 38: C7–51
6. Hohenberg PC, Halperin BI. 1977. *Rev. Mod. Phys.* 49:435–79
7. Gunton JD, Miguel MS, Sahni PS. 1983. The dynamics of first-order phase transitions. In *Phase Transitions and Critical Phenomena*, ed. C Domb, JL Lebowitz, pp. 267–466. New York: Academic
8. Elder KR, Grant M, Provatas N, Kosterlitz JM. 2001. *Phys. Rev. E* 64:021604
9. Langer JS. 1986. Models of pattern formation in first-order phase transitions. In *Directions in Condensed Matter Physics*, ed. G Grinstein, G Mazenko, pp. 165–86. Singapore: World Scientific
10. Fix GJ. 1983. In *Free Boundary Problems: Theory and Applications*, ed. A Fasano, M Primicerio, Boston: Piman. 580 pp.
11. Collins JB, Levine H. 1985. *Phys. Rev. B* 31:6119
12. Karma A. 2001. Phase field methods. In *Encyclopedia of Materials Science and Technology*, ed. KHJ Buschow, RW Cahn, MC Flemings, BB Ilschner, EJ Kramer, et al. pp. 6873–86. Oxford, UK: Elsevier
13. Ode M, Kim SG, Suzuki T. 2001. *ISIJ Int.* 41:1076–82
14. Chen LQ, Wang YZ. 1996. *J. Miner. Met. Mater. Soc.* 48:13–18
15. Wang YZ, Chen LQ. 1999. Simulation of

microstructure evolution. In *Methods in Materials Research*, ed. EN Kaufmann, R Abbaschian, A Bocarsly, CL Chien, D Dollimore, et al., pp. 2a.3.1; 2a.3.23. New York: Wiley & Sons
16. Chen LQ, Yang W. 1994. *Phys. Rev. B* 50: 15752–56
17. Steinbach I, Pezzolla F, Nestler B, Seesselberg M, Prieler R, et al. 1996. *Physica D* 94:135–47
18. Lusk MT. 1999. *Proc. R. Soc. London Ser. A.* 455:677–700
19. Kobayashi R, Warren JA, Carter WC. 2000. *Physica D* 140:141–50
20. Li YL, Hu SY, Liu ZK, Chen LQ. 2001. *Appl. Phys. Lett.* 78:3878–80
21. Leo PH, Johnson WC. 2001. *Acta Mater.* 49:1771–87
22. Lu W, Suo Z. 2001. *J. Mech. Phys. Solids* 49:1937–50
23. Aranson IS, Kalatsky VA, Vinokur VM. 2000. *Phys. Rev. Lett.* 85:118–21
24. Karma A, Kessler DA, Levine H. 2001. *Phys. Rev. Lett.* 87:045501
25. Kassner K, Misbah C, Muller J, Kappey J, Kohlert P. 2001. *J. Cryst. Growth* 25:289–93
26. Kassner K, Misbah C, Muller J, Kappey J, Kohlert P. 2001. *Phys. Rev. E* 63:036117
27. Leonard F, Desai RC. 1998. *Phys. Rev. B* 58:8277–88
28. Hu SY, Chen LQ. 2001. *Acta Mater.* 49: 463–72
29. Wang YU, Jin YM, Cuitino AM, Khachaturyan AG. 2001. *Appl. Phys. Lett.* 78: 2324–26
30. Mahadevan M, Bradley RM. 1999. *Physica D* 126:201–13
31. Bhate DN, Kumar A, Bower AF. 2000. *J. Appl. Phys.* 87:1712–21
32. Wu K, Morral JE, Wang Y. 2001. *Acta Mater.* 49:3401–8
33. Oono Y, Puri S. 1988. *Phys. Rev. A* 38: 434–53
34. Blowey JF, Elliott CM. 1991. *Eur. J. Appl. Math.* 2:233–79
35. Caginalp G, Chen X. 1992. Phase field equations in the singular limit of sharp interface problems. In *On the Evolution of Phase Boundaries*, ed. ME Gurtin, GB McFadden, 43:1–27. New York: Springer-Verlag
36. Lai ZW. 1990. *Phys. Rev. B* 41:9239–56
37. Braun RJ, Cahn JW, McFadden GB, Rushmeier HE, Wheeler AA. 1997. *Acta Mater.* 46:1–12
38. Braun RJ, Cahn JW, McFadden GB, Wheeler AA. 1997. *Philos. Trans. R. Soc. London Ser. A* 355:1787–833
39. Wang Y, Banerjee D, Su CC, Khachaturyan AG. 1998. *Acta Mater.* 46:2983–3001
40. Li DY, Chen LQ. 1998. *Acta Mater.* 47: 247–57
41. Devonshire AF. 1954. *Philos. Mag. Suppl.* 3:85
42. Nambu S, Sagala DA. 1994. *Phys. Rev. B* 50:5838–47
43. Hu HL, Chen LQ. 1998. *J. Am. Ceram. Soc.* 81:492–500
44. Hu HL, Chen LQ. 1997. *Mater. Sci. Eng. A* 238:182–91
45. Landau LD. 1937. *J. Exp. Theor. Phys.* 7: 19
46. Khachaturyan AG. 1983. *Theory of Structural Transformations in Solids*. New York: Wiley & Sons.
47. Kobayashi R. 1993. *Physica D* 63:410
48. Wheeler AA, Murray BT, Schaefer RJ. 1993. *Physica D* 66:243–62
49. Eggleston JJ, McFadden GB, Voorhees PW. 2001. *Physica D* 150:91–103
50. Taylor JE, Cahn JW. 1998. *Physica D* 112:381–411
51. Abinandanan TA, Haider F. 2001. *Philos. Mag. A* 81:2457–79
52. Onuki A. 1989. *J. Phys. Soc. Jpn.* 58: 3065–68
53. Chen LQ. 2000. On the elastic field coupling in the diffuse-interface modeling of coherent microstructures. In *Phase Transformations and Evolution in Materials*, ed. PEA Turchi, A Gonis, pp. 209–20. Warrendale, PA: Miner. Met. Mater. Soc.
54. Khachaturyan AG, Shatalov GA. 1969. *Sov. Phys. Solid State* 11:118–23

55. Nishimori H, Onuki A. 1990. *Phys. Rev. B* 42:980–83
56. Sagui C, Orlikowski D, Somoza A, Roland C. 1998. *Phys. Rev. E.* 58:569–77
57. Hu SY, Chen LQ. 2001. *Acta Mater.* 49: 1879–90
58. Leo PH, Lowengrub JS, Hou HJ. 1998. *Acta Mater.* 61:2113–30
59. Zhu JZ, Chen LQ, Shen J. 2001. *Model. Simulat. Mater. Sci. Eng.* 9:499–511
60. Semenovskaya S, Khachaturyan AG. 1998. *Ferroelectrics* 206:157–80
61. Wang Y, Chen LQ, Khachaturyan AG. 1993. *Acta Metall. Mater.* 41:279–96
62. Fan D, Chen LQ. 1995. *J. Am. Ceram. Soc.* 78:769–73
63. Wang YZ, Chen LQ, Khachaturyan AG. 1996. *J. Am. Ceram. Soc.* 79:987–91
64. Chen LQ, Shen J. 1998. *Comput. Phys. Commun.* 108:147–58
65. Zhu JZ, Chen LQ, Shen J, Tikare V. 1999. *Phys. Rev. E* 60:3564–72
66. Shen J. 1994. *SIAM J. Sci. Comput.* 15: 1489–505
67. Shen J. 1995. *SIAM J. Sci. Comput.* 16: 74–87
68. Provatas N, Goldenfeld N, Dantzig J. 1998. *Phys. Rev. Lett.* 80:3308–11
69. Jeong JH, Goldenfeld N, Dantzig JA. 2001. *Phys. Rev. E.* 64:041602
70. Plapp M, Karma A. 2000. *J. Comput. Phys.* 165:592–619
71. Karma A, Rappel WJ. 1999. *Phys. Rev. E* 60:3614–25
72. Bragard J, Karma A, Lee YH, Plapp M. 2001. *Interface Sci.* Preprint
73. Anderson DM, McFadden GB, Wheeler AA. 1998. *Annu. Rev. Fluid Mech.* 30: 139–65
74. Denniston C, Yeomans JM. 1999. *Phys. Chem. Chem. Phys.* 1:2157–61
75. Jacqmin D. 1999. *J. Comput. Phys.* 155: 96–127
76. Folch R, Casademunt J, Hernandez-Machado A, Ramirez-Piscina L. 1999. *Phys. Rev. E* 60:1724–33
77. Beckermann C, Diepers HJ, Steinbach I, Karma A, Tong X. 1999. *J. Comput. Phys.* 154:468–96
78. Diepers HJ, Beckermann C, Steinbach I. 1999. *Acta Mater.* 47:3663–78
79. Pismen LM, Pomeau Y. 2000. *Phys. Rev. E* 62:2480–92
80. Nestler B, Wheeler AA, Ratke L, Stocker C. 2000. *Physica D* 141:133–54
81. Ganesan V, Brenner H. 2000. *Proc. R. Soc. London Ser. A* 456:731–803
82. Boettinger WJ, Coriell SR, Greer AL, Karma A, Kurz W, et al. 2000. *Acta Mater.* 48:43–70
83. Lo TS, Karma A, Plapp M. 2001. *Phys. Rev. E* 63:031504
84. Tong X, Beckermann C, Karma A, Li Q. 2001. *Phys. Rev. E* 63:061601
85. Wheeler AA, Boettinger WJ, McFadden GB. 1992. *Phys. Rev. A* 45:7424–39
86. Caginalp G, Xie W. 1993. *Phys. Rev. E* 48:1897–909
87. Boettinger WJ, Wheeler AA, Murray BT, McFadden GB. 1994. *Mater. Sci. Eng. A* 178:217–23
88. Warren JA, Boettinger WJ. 1995. *Acta Metall. Mater.* 43:689–703
89. Bi ZQ, Sekerka RF. 1998. *Physica A* 261:95–106
90. Tiaden J, Nestler B, Diepers HJ, Steinbach I. 1998. *Physica D* 115:73–86
91. Ahmad NA, Wheeler AA, Boettinger WJ, McFadden GB. 1998. *Phys. Rev. E* 58:3436–50
92. Charach C, Fife PC. 1999. *J. Cryst. Growth* 199:1267–74
93. Kim SG, Kim WT, Suzuki T. 1999. *Phys. Rev. E* 60:7186–97
94. Muller I. 2001. *Int. J. Solids Struct.* 38: 1105–13
95. Galenko P. 2001. *Phys. Lett. A* 287:190–97
96. Kim WT, Kim SG, Lee JS, Suzuki T. 2001. *Metall. Mater. Trans. A* 32:961–69
97. Wheeler AA, McFadden GB, Boettinger WJ. 1996. *Proc. R. Soc. London Ser. A.* 452:495–525
98. Plapp M, Karma A. 1999. *Phys. Rev. E* 60: 6865–89

99. Drolet F, Elder KR, Grant M, Kosterlitz JM. 2000. *Phys. Rev. E* 61:6705–20
100. Nestler B, Wheeler AA. 2000. *Physica D* 138:114–33
101. Lee JS, Kim SG, Kim WT, Suzuki T. 1999. *ISIJ Int.* 39:730–36
102. Tiaden J. 1999. *J. Cryst. Growth* 199: 1275–80
103. Bottger B, Grafe U, Ma D, Fries SG. 2000. *Mater. Sci. Technol.* 16:1425–28
104. Ode M, Lee JS, Kim SG, Kim WT, Suzuki T. 2000. *ISIJ Int*. 40:870–76
105. Cha PR, Yeon DH, Yoon JK. 2001. *Acta Mater.* 49:3295–307
106. Grafe U, Bottger B, Tiaden J, Fries SG. 2000. *Scripta Mater.* 42:1179–86
107. Grafe U, Bottger B, Tiaden J, Fries SG. 2000. *Model. Simul. Mater. Sci. Eng.* 8: 871–79
108. Loginova I, Amberg G, Agren J. 2001. *Acta Mater.* 49:573–81
109. McFadden GB, Wheeler AA, Braun RJ, Coriell SR, Sekerka RF. 1993. *Phys. Rev. E* 48:2016–24
110. Fried E. 1997. *Continuum Mech. Thermodyn.* 9:33–60
111. Fabbri M, Voller VR. 1997. *J. Comput. Phys.* 130:256–65
112. Garcke H, Nestler B, Stoth B. 1998. *Physica D* 115:87–108
113. Karma A, Rappel WJ. 1998. *Phys. Rev. E* 57:4323–49
114. McFadden GB, Wheeler AA, Anderson DM. 2000. *Physica D* 144:154–68
115. Anderson DM, McFadden GB, Wheeler AA. 2001. *Physica D* 151:305–31
116. Hariharan SI, Young GW. 2001. *SIAM J. Appl. Math.* 62:244–63
117. Karma A, Rappel WJ. 1996. *Phys. Rev. E* 53:R3107–20
118. Ode M, Lee JS, Suzuki T, Kim SG, Kim WT. 1999. *ISIJ Int.* 39:149–53
119. Karma A. 2001. *Phys. Rev. Lett.* 87: 115701
120. Rogers TM, Elder KR, Desai RC, 1988. 1988. *Phys. Rev. B* 37:9638–49
121. Venugopalan V, Chen LQ. 2000. 3D simulation of coarsening of gamma-prime precipitates in a Ni-Al alloy. In *Nucleation and Growth Processes in Materials*, ed. A Gonis, PEA Turchi, AJ Ardell, pp. 327–32. Boston: Mater. Res. Soc.
122. Vaithyanathan V, Chen LQ. 2000. *Scripta Mater.* 42:967–73
123. Wen YH, Wang Y, Bendersky LA, Chen LQ. 2000. *Acta Mater.* 48:4125–35
124. Proville L, Finel A. 2001. *Phys. Rev. B* 64:054104
125. Wang YZ, Wang HY, Chen LQ, Khachaturyan AG. 1993. *J. Am. Ceram. Soc.* 76: 3029–33
126. Semenovskaya S, Zhu YM, Suenaga M, Khachaturyan AG. 1993. *Phys. Rev. B* 47: 12182–89
127. Fan DN, Chen LQ. 1995. *J. Am. Ceram. Soc.* 78:1680–86
128. Le Bouar Y, Loiseau A, Khachaturyan AG. 1998. *Acta Mater.* 46:2777–88
129. Le Bouar Y, Khachaturyan AG. 2000. *Acta Mater.* 48:1705–17
130. Wen YH, Wang Y, Chen LQ. 1999. *Acta Mater.* 47:4375–86
131. Cahn JW, Han SC, McFadden GB. 1999. *J. Stat. Phys.* 95:1337–60
132. Wen YH, Wang Y, Chen Q. 2000. *Philos. Mag. A* 80:1967–82
133. Wen YH, Chen LQ, Hazzledine PM, Wang Y. 2001. *Acta Mater.* 49:2341–53
134. Semenovskaya S, Khachaturyan AG. 1998. *J. Appl. Phys.* 83:5125–36
135. Wang Y, Khachaturyan AG. 1997. *Acta Mater.* 45:759–73
136. Jin YM, Artemev A, Khachaturyan AG. 2001. *Acta Mater.* 49:2309–20
137. Artemev A, Jin Y, Khachaturyan AG. 2001. *Acta Mater.* 49:1165–77
138. Li DY, Chen LQ. 1998. *Acta Mater.* 46: 639–49
139. Li DY, Chen LQ. 1998. *Acta Mater.* 46: 2573–85
140. Artemev A, Wang Y, Khachaturyan AG. 2000. *Acta Mater.* 48:2503–18
141. Chen LQ. 1994. *Mod. Phys. Lett. B* 7: 1857–81

142. Wen YH, Wang Y, Chen LQ. 2001. *Acta Mater.* 49:13–20
143. Fan DA, Chen LQ. 1997. *Philos. Mag. Lett.* 75:187–96
144. Fan DN, Geng CW, Chen LQ. 1997. *Acta Mater.* 45:1115–26
145. Fan D, Chen LQ. 1997. *Acta Mater.* 45: 611–22
146. Krill CE, Chen LQ. 2002. *Acta Mater.* In press
147. Garcke H, Nestler B, Stoth B. 1999. *SIAM J. Appl. Math.* 60:295–315
148. Nestler B. 1999. *J. Cryst. Growth* 204: 224–28
149. Garcke H, Nestler B. 2000. *Math. Models Methods Appl. Sci.* 10:895–921
150. Warren JA, Carter WC, Kobayashi R. 1998. *Physica A* 261:159–66
151. Kobayashi R, Warren JA, Carter WC. 1998. *Physica D* 119:415–23
152. Warren JA, Kobayashi R, Carter WC. 2000. *J. Cryst. Growth* 211:18–20
153. Lobkovsky AE, Warren JA. 2001. *Phys. Rev. E* 63:051605
154. Lobkovsky AE, Warren JA. 2001. *J. Cryst. Growth* 225:282–88
155. Kazaryan A, Wang Y, Dregia SA, Patton BR. 2000. *Phys. Rev. B* 61:14275–78
156. Kazaryan A, Wang Y, Dregia SA, Patton BR. 2001. *Phys. Rev. B* 63:184102
157. Cahn JW, Fife P, Penrose O. 1997. *Acta Mater.* 45:4397–413
158. Fan D, Chen SP, Chen LQ. 1999. *J. Mater. Res.* 14:1113–23
159. Fan DN, Chen LQ, Chen SP, Voorhees PW. 1998. *Comput. Mater. Sci.* 9:329–36
160. Fan DN, Chen SP, Chen LQ, Voorhees PW. 2001. *Acta Mater.* In press
161. Chen LQ, Fan DA. 1996. *J. Am. Ceram. Soc.* 79:1163–68
162. Danan F, Chen LQ. 1997. *J. Am. Ceram. Soc.* 80:1773–80
163. Fan DN, Chen LQ. 1997. *Acta Mater.* 45: 3297–310
164. Fan DA, Chen LQ. 1997. *Scripta Mater.* 37:233–38
165. Fan D, Chen LQ. 1997. *Acta Mater.* 45: 4145–54
166. Li YL, Hu SY, Liu ZK, Chen LQ. 2001. *Acta Mater.* In press
167. Suo Z, Lu W. 2000. *J. Mech. Phys. Solids.* 48:211–32
168. Karma A, Plapp M. 1998. *Phys. Rev. Lett.* 81:4444–47
169. Muller J, Grant M. 1999. *Phys. Rev. Lett.* 82:1736–39
170. Kassner K, Misbah C. 1999. *Europhys. Lett.* 46:217–23
171. Cottrell AH. 1948. Effect of solute atoms on the behaviour of dislocations. In *Report of a Conference on Strength of Solids*, ed. NF Mott, pp. 30–38. London: Phys. Soc.
172. Cahn JW. 1957. *Acta Metall.* 5:169
173. Hu SY, Chen LQ. 2001. *Comput. Mater. Sci.* 49: 463–72
174. Rodney D, Le Bouar Y, Finel A. 2001. *Acta Mater.* In press
175. Wang YU, Jin UM, Cuitino AM, Khachaturyan AG. 2001. *Acta Mater.* 49:1847–57
176. Wang YU, Jin YM, Cuitino AM, Khachaturyan AG. 2001. *Philos. Mag. Lett.* 81: 385–93
177. Jin YM, Khachaturyan AG. 2001. *Philos. Mag. Lett.* 81:607–16
178. Deleted in proof
179. Mahadevan M, Bradley RM. 1999. *Phys. Rev. B* 59:11037–46
180. Tadmor EB, Phillips R, Ortiz M. 1996. *Langmuir* 12:4529–34
181. Abraham FF, Broughton JQ, Bernstein N, Kaxiras E. 1998. *Europhys. Lett.* 44:783–87
182. Abraham FF, Broughton JQ, Bernstein N, Kaxiras E. 1998. *Comput. Phys.* 12:538–46
183. Phillips R. 1998. *Curr. Opin. Solid State Mater. Sci.* 3:526–32
184. Rudd RE, Broughton JQ. 1998. *Phys. Rev. B* 58:R5893–96
185. Broughton JQ, Abraham FF, Bernstein N, Kaxiras E. 1999. *Phys. Rev. B.* 60:2391–403

186. Rudd RE, Broughton JQ. 2000. *Phys. Status Solidi B* 217:251–91
187. Vaithynanathan V, Woverton C, Chen LQ. 2001. *Phys. Rev. Lett.* In press
188. Chen LQ, Wolverton C, Vaithyananthan V, Liu ZK. 2001. *MRS Bull.* 26:197–202
189. Hoyt JJ, Sadigh B, Asta M, Foiles SM. 1999. *Acta Mater.* 47:3181–77
190. Hoyt JJ, Asta M, Karma A. 2001. *Phys. Rev. Lett.* 86:5530–33
191. Zhu JZ, Liu ZK, Vaithyanathan V, Chen LQ. 2001. *Scripta Mater.* In press

Figure 1 A snapshot of a three-dimensional dendrite in pure Ni with a cubic interfacial energy anisotropy obtained from a phase-field simulation with thermal noises (72) (courtesy of A. Karma). The interfacial energy and mobility anisotropies were obtained from atomistic simulations, and they are matched to the kinetic coefficients in the phase-field model using a thin-interface analysis.

Annual Review of Materials Research
Volume 32, 2002

CONTENTS

COMPUTATIONAL MATERIALS RESEARCH